INTERNATIONAL JOURNAL FOR NUMERICAL METHODS IN FLUIDS
Int. J. Numer. Meth. Fluids 2007; **55**:81–101
Published online 21 February 2007 in Wiley InterScience (www.interscience.wiley.com). DOI: 10.1002/fld.1441

Solution of depth-averaged tidal currents in Persian Gulf on unstructured overlapping finite volumes

Saeed-Reza Sabbagh-Yazdi*,†,‡, Mohammad Zounemat-Kermani§ and Ali Kermani¶

Department of Civil Engineering, K.N. Toosi University of Technology, ValiAsr St. Tehran, Iran

SUMMARY

Hydrodynamic simulation of tidal currents in Persian Gulf due to tidal fluctuations in Hurmoz strait and inflow for Arvand River is presented in this paper and tidal constituents of M2 and K1 are attained. The mathematical model utilized consists of depth-averaged equations of continuity and motion in two-dimensional horizontal plane which considers hydrostatic pressure distribution. The effect of evaporation is considered in the continuity equation and the effects of bed slope and friction, as well as the Coriolis effects are considers in two equations of motion. The cell vertex finite volume method is applied for converting the governing equations into discrete forms for unstructured overlapping control volumes. Using unstructured triangular meshes provides great flexibility for modelling of complex geometries in the real world flow domain. The accuracy of the developed flow solver is assessed using two test cases. Firstly, the results of the hydrodynamic model for fluctuating flow on the variable bed slope are compared with available analytical solution. Secondly, in order to simulate circulating flow patterns the numerical results are compared with the reported data in the literature for deep flow in a canal with sudden expansion. Finally, the performance of the computer model to simulate tidal flow in a geometrically complex domain is examined by simulation of tidal currents in the Persian Gulf and computing tidal constituents. Copyright © 2007 John Wiley & Sons, Ltd.

Received 31 August 2005; Revised 2 December 2006; Accepted 6 December 2006

KEY WORDS: tidal constituents; Persian Gulf; unstructured mesh; overlapping finite volumes

1. INTRODUCTION

The computer simulation of complicated marine environment problems have become one of the interesting areas of research by development of efficient and accurate numerical methods suitable

*Correspondence to: Saeed-Reza Sabbagh-Yazdi, Department of Civil Engineering, K.N. Toosi University of Technology, ValiAsr St. Tehran, Iran.
†E-mail: syazdi@kntu.ac.ir
‡Assistant Professor.
§Ph.D. Student.
¶Graduate Student.

for the complex flow domain. The control over properties and behaviour of fluid flow and relative parameters are the advantages offered by computational fluid dynamics (CFD) which make it suitable for the simulation of the applied engineering problems.

Water free surface treatment is one of the major difficulties in numerical solution of three-dimensional water flow patterns. Some of the models apply a normalized coordinate (sigma coordinate) system in the vertical direction to solve three-dimensional flow equations. Three-dimensional flow solvers are computationally costly. The Princeton ocean model (POM) is one of these models, which uses finite difference method for solving flow equations on multi-block grids [1].

Multi-layer flow solvers may produce some information about vertical variations of horizontal velocity components using normalized coordinate systems in vertical direction. But, they are based on layered averaged hypotheses, and thus, their results are two-dimensional multi-layered and no accurate prediction of vertical velocity component can be obtained in spite of their computational cost [2].

Some numerical workers have tried to extract the vertical structure of the current solution in the particular zones of interest where considerable depth variation of horizontal velocity components exists [3, 4]. Such approximated three-dimensional results are achieved by solving a one-dimensional hydrodynamic equation locally (using normalized coordinate system in vertical direction) after computation of depth-averaged horizontal velocity components [5]. However, such an algorithm does not produce perfect three-dimensional results over the entire solution domain.

Two-dimensional depth-averaged models are well established computationally efficient models where the vertical component of the velocities are not significant in comparison with the horizontal component, and therefore, the vertical profile of the current is not of major interest. However, for the cases where high pressure gradient due to tidal elevations are balanced by the bottom stresses or for the cases where extensive amount of mixing provides a well-mixed water column, using two-dimensional depth-averaged model may be justified [6–9].

Some numerical workers have used finite element method, such as BELLAMY which applies a depth-averaged, nonlinear, time-stepping finite element model [7, 10]. Some other models like OTIS uses finite difference method for time stepping repeated solution of the linearized shallow water equations, and the adjoint of this system [11].

Recently, some models were established for coastal ocean and estuary environment flow problems on the basis of finite volume method. The finite volume community ocean model (FVCOM) employs unstructured non-overlapping cell vertex triangular control volumes for the solution of shallow water equations in the horizontal plane. This model uses finite differences for solving the equations in the vertical direction, using a sigma-coordinate system [12].

On the other hand, several models for the hydrodynamic behaviour of the Persian Gulf are reported in the literature. Some of the numerical models of the Persian Gulf have used two-dimensional depth-averaged hydrodynamic equations in Cartesian coordinates system [5, 13–15]. In order to get more accurate results, in some modelling efforts the two-dimensional depth-averaged equations are transformed into spherical coordinates system [16–19]. Most of these models use finite difference method for solving the utilized hydrodynamic equations.

The main goal of the present work is to test numerical analyser for scientific and industrial requirements (NASIR) hydrodynamic shallow water flow solver model for prediction of the Persian Gulf currents on unstructured cell vertex overlapping finite volumes. In this flow solver in order to improve the shortcomings of the computations on unstructured meshes, some efficiency improvement techniques such as multi-stage time stepping, residual smoothing and edge-base

DOI: 10.1002/fld

algorithm are employed. Application of these techniques provokes major differences with previous hydrodynamic models used for tidal flow predictions.

2. PERSIAN GULF CHARACTERISTICS

Vast areas of the Persian Gulf (with 1000 km length, 340 km maximum width and less than 0.1 km maximum depth) is shallow and one-third of the region has more than 0.04 km depth. Hence, it seems that such conditions match with most areas of the Persian Gulf region. Figure 1 shows the general location of the gulf and marks major islands and locations which were mentioned in the present study.

The necessary condition for using shallow water equations is described as $h/l < \frac{1}{20}$, where h presents water depth and l stands for wave length. The wave length equation is determined as $l = (gT^2/2\pi)\tanh(2\pi h/l)$ (where T is the period for tidal waves) considering maximum depth the Persian Gulf (equals to 100 m), the maximum tidal oscillations (3 m) and astronomical tidal constituents $M2$, $S2$, $K1$, $O1$ (which presents the minimum tidal period of $S_2 = 12$ h); the calculated wave length in Persian Gulf is about 45 km [20]. Therefore, the value h/l is less than 0.0022 for Persian Gulf which is far less than $\frac{1}{20}$, this fact justifies application of depth-averaged shallow water equations for numerical modelling of Persian Gulf. Because of this shallowness of Persian Gulf, several numerical workers have applied the set of shallow water equations for simulation of tidal currents in Persian Gulf [21–23].

It worth noting that the Hurmoz strait is the major inflow boundary of Persian Gulf from which annually 295 km^3 of water enters the Persian Gulf domain due to considerable evaporations from the water surface. However, the water surface fluctuations due to oceanic tides are the main factor for forming flow patterns in the Persian Gulf region.

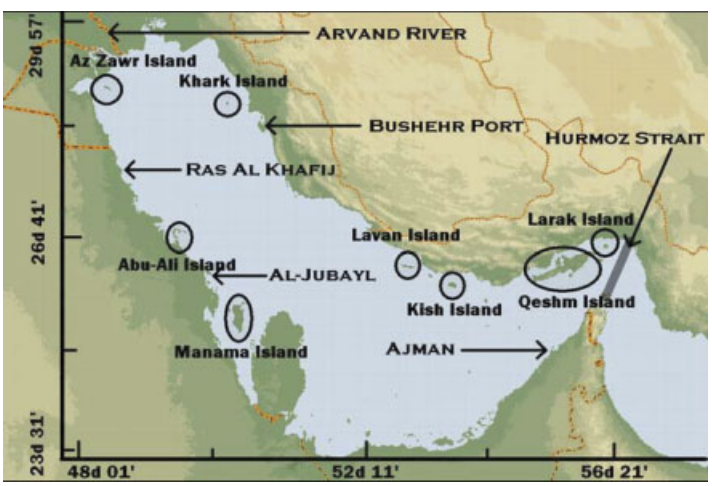

Figure 1. The Persian Gulf map (with geographical coordinates) in which the location of Hurmoz strait, Arvand River, Bushehr, Ajman and Ras-Al-Khafij ports and major islands are marked.

DOI: 10.1002/fld

The tidal fluctuations for some specific points can be obtained from Admiralty tide table predictions which are computed by harmonic analysis and adapted with regional conditions [24]. The Hurmoz strait (as the tidal boundary of the Persian Gulf) is one of these points. However, lack of information about tidal fluctuations at other points motivates development and application of hydrodynamic models.

3. HYDRODYNAMIC EQUATIONS

The depth-integrated continuity and momentum equations of free surface water flow are

$$\frac{\partial h}{\partial t}+\frac{\partial hu}{\partial x}+\frac{\partial hv}{\partial y}=Q_z \tag{1}$$

$$\frac{\partial hu}{\partial t}+\frac{\partial huu}{\partial x}+\frac{\partial hvu}{\partial y}=-gh\frac{\partial z_s}{\partial x}+\left(\frac{\partial hT_{xx}}{\partial x}+\frac{\partial hT_{xy}}{\partial y}\right)-\left(\frac{\tau_{bx}}{\rho_w}\right)+f_{cx} \tag{2}$$

$$\frac{\partial hv}{\partial t}+\frac{\partial huv}{\partial x}+\frac{\partial hvv}{\partial y}=-gh\frac{\partial z_s}{\partial y}+\left(\frac{\partial hT_{yx}}{\partial x}+\frac{\partial hT_{yy}}{\partial y}\right)-\left(\frac{\tau_{by}}{\rho_w}\right)+f_{cy} \tag{3}$$

In the above equations, t is the time, x and y the horizontal Cartesian coordinates, h the flow depth, u and v the depth-averaged flow velocities in x and y directions, Q_z the rainfall–evaporation volume per unit area of water surface, z_s the water surface elevation ($z_s=h+z_b$), and g the gravitational acceleration.

Bed friction global stresses in x and y, $\tau_{bx}=\rho_w C_f u|U|$ and $\tau_{by}=\rho_w C_f v|U|$, directions are calculated using $C_f=gn^2/h^{1/3}$ (n represents manning coefficient).

Coriolis forces due to earth rotation $f_{cx}=hv\omega\sin\phi$ and $f_{cy}=-hu\omega\sin\phi$ in which ω is the earth angular velocity and ϕ the geographical latitude [25].

The depth-integrated horizontal turbulent stress is modelled using T_{xx}, T_{xy}, T_{yx} and T_{yy}:

$$T_{xx}=2(\nu+\nu_t)\frac{\partial u}{\partial x}-\frac{2}{3}\kappa \tag{4a}$$

$$T_{xy}=T_{yx}=(\nu+\nu_t)\left(\frac{\partial u}{\partial y}+\frac{\partial v}{\partial x}\right) \tag{4b}$$

$$T_{xx}=2(\nu+\nu_t)\frac{\partial v}{\partial y}-\frac{2}{3}\kappa \tag{4c}$$

where ν is the kinematics viscosity of water, ν_t the eddy viscosity due to turbulent, and κ the turbulent energy, which is dropped from the equations when zero-equation turbulence models are used. Several turbulence models including depth-averaged parabolic eddy viscosity model [26], sub-grid-scale trace-free model [27], sub-depth-scale mixing length one equation model for turbulent energy [28], standard κ–ε two equations model for free surface flow [29] and the renormalization group κ–ε two equations model can be used for computation of eddy viscosity parameter [23].

Well-known two-equation κ–ε turbulent model is reported to be a suitable turbulent model for three-dimensional applications and its two-dimensional depth-averaged version is used by several numerical workers. However, in spite of the excessive computational work load of κ–ε

DOI: 10.1002/fld

two-dimensional depth-averaged model, it does not produce much better results than zero-equation models [23]. Perhaps, the assumptions of negligible variation in vertical direction for horizontal velocities and no vertical velocity component in shallow flow models do not match the basis of κ–ε turbulent models (production and dissipation of kinetic energy due to three-dimensional turbulent eddies). On the other hand, the zero-equation models which globally consider the effects of bed friction (*via* shear velocity) provide better evaluations for global dissipative effect of turbulence effects which mainly originate from the bed roughness in shallow water flow modelling [30].

In the present work, the widely used depth-averaged parabolic turbulent model is applied, in which the eddy viscosity parameter is computed by the algebraic formulation $\nu_t = \theta h U_*$. In this formulation the bed friction velocity is defined as $U_* = [C_f(u^2+v^2)]^{0.5}$ and the empirical coefficient θ is advised between 0.3 and 1.0. This turbulence model is known suitable for depth-averaged equations and has been used in some similar applications [30, 31].

4. NUMERICAL FORMULATIONS

Considering the governing equations in form of an advection–diffusion type equation, W represents the variables using h flow depth, hu and hv the horizontal components of velocity. G^c and F^c are vectors of convective fluxes, while, G^d and F^d are vectors of diffusive fluxes of W in x and y directions, respectively. The vector S contains the sources and sinks of the governing equations covering all algebraic terms.

$$\frac{\partial W}{\partial t} + \left(\frac{\partial F^c}{\partial x} + \frac{\partial G^c}{\partial y}\right) = \left(\frac{\partial F^d}{\partial x} + \frac{\partial G^d}{\partial y}\right) + S \tag{5}$$

The governing equations are discretized by the application of cell vertex (overlapping) scheme of the finite volume method [32]. Considering proper techniques to convert diffusive fluxes into discrete form and source term treatment, this method results in the following formulation:

$$W_i^{t+\Delta t} = W_i^t - \frac{\Delta t}{\Omega_i} \sum_{k=1}^{N_{\text{sides}}} [(\overline{F}^c \Delta y - \overline{G}^c \Delta x) - (F^d \Delta y - G^d \Delta x)]_k^t + \frac{\Delta t}{3} S_i^t \tag{6}$$

where W_i represents conserved variables at the centre of control volume Ω_i. $\overline{F}^c$ and $\overline{G}^c$ are the mean values of convective fluxes on the control volume boundary sides. S_i^t is the source term which covers volumetric evaporations and body forces. The diffusive fluxes F^d and G^d are computed using a discrete formula of contour integral around the centre of the control volume boundary sides (using an auxiliary control volume).

Note that, the unstructured overlapping control volumes Ω_i are formed by gathering triangles meeting a computational node (Figure 2). Using cell vertex control volumes, provides direct computation of flow variables at nodal points. Unlike cell centre schemes, cell vertex scheme solves flow variables directly at computational nodes and there is no need for reconstruction of unknowns from the computed value at the cells centroid or calculating flow variables at auxiliary points. Hence, by using overlapping cell vertex scheme, computational work load is saved with no accuracy degradation.

In other words, by using overlapping schemes, the fluxes at control volumes boundaries can be directly computed by means of variables at computational nodes, while the non-overlapping

DOI: 10.1002/fld

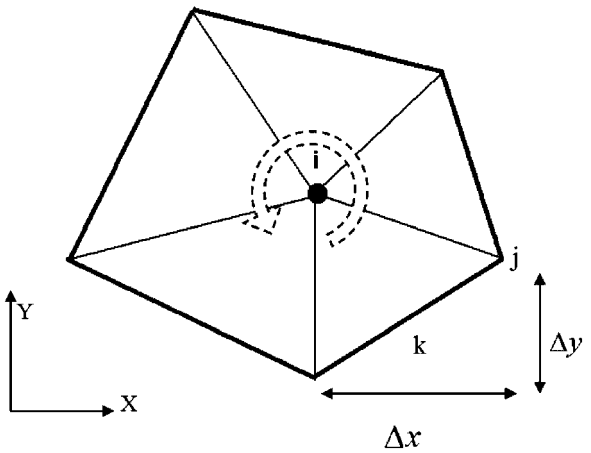

Figure 2. A cell vertex overlapping control volume formed by gathering triangular cells.

schemes requires the value of flow variables in some points within cells. Thereafter, computational work load of overlapping schemes are less than non-overlapping schemes.

The residual term, $R(W_i) = \sum_{k=1}^{N_{\text{sides}}} [(\overline{F}^c \Delta y - \overline{G}^c \Delta x) - (F^d \Delta y - G^d \Delta x)]_k^t$, consists of convective and diffusive parts. In smooth parts of the flow domain, where there is no strong gradient of flow parameters, the convective part of the residual term dominates. Since, in the explicit computation of convection dominated flow there is no mechanism to damp out the numerical oscillations, it is necessary to apply numerical techniques to overcome instabilities with minimum accuracy degradation. In the present work, the artificial dissipation terms suitable for the unstructured meshes are used to stabilize the numerical solution procedure. In order to damp unwanted numerical oscillations, a fourth-order artificial dissipation term, $D(W_i) = \varepsilon \sum_{j=1}^{N_{\text{edges}}} \lambda_{ij} (\nabla^2 W_j - \nabla^2 W_i)$, is added to the above algebraic formula in which λ_{ij} is a scaling factor and is computed using the maximum value of the spectral radii of every edge connected to node i ($\frac{1}{256} \leqslant \varepsilon \leqslant \frac{3}{256}$). Here, the Laplacian operator at every node i, $\nabla^2 W_i = \sum_{j=1}^{N_{\text{edges}}} (W_j - W_i)$, is computed using the variables W at two end nodes of edges (meeting node i). The revised formula, which preserves the accuracy of the numerical solution, is given in the following relation:

$$W_i^{t+\Delta t} = W_i^t - \frac{\Delta t}{\Omega_i} \{R(W_i^t) - D(W_i^t)\} + \frac{\Delta t}{3} S_i^t \tag{7}$$

Δt is the minimum time step of the domain proportional to the minimum mesh spacing and maximum wave speed of the convective homogonous equations.

5. EFFICIENCY IMPROVEMENT

In order to improve computational efficiency of the developed model, some of the techniques which were applied in the CFD models on unstructured meshes, are adopted in this work.

DOI: 10.1002/fld

5.1. Multi-stage time stepping

The multi-stage time stepping increases the temporal accuracy of the overall scheme. Therefore, using Runge–Kutta method is a common practice in numerical solution of time dependent problems to provide stability of the explicit schemes and increase their time-wise accuracy [33]. In present free surface flow model, a three-stage Runge–Kutta scheme (with coefficients 0.6, 0.6 and 1.0), which damps high frequency errors, is used for stabilizing the explicit time stepping process.

5.2. Residual smoothing

Implicit smoothing the computed residual at each computational stage increases the stability of the computations. The idea behind this scheme is to replace the residual at one point of the flow field with a smoothed or weighted average of residuals at the neighbouring points. In the present work, two iterations of the implicit residual smoothing technique are used [34].

5.3. Edge base algorithm

Using the unstructured meshes with irregular distribution of node numbering require direct addressing of the mesh data (including coordinate of nodes and element connectivity) which is saved in a certain part of the computer memory. Hence, solution algorithms, which utilize unstructured meshes, suffer from shortcoming in terms of computational efficiency due to the communication between memory and central processing unit of the computer. This problem is more pronounced if the computational process needs explicit iteration and fine mesh spacing (which requires small values of computational steps).

On the other hand, each internal edge is shared between two neighbouring control volumes. Therefore, in each computational loop, not only the coordinates of the two end points of internal edges, but also the convective (and diffusive) fluxes are used twice for computations. Furthermore, in this work, the computation of the fluxes and dissipative operators are performed using edges connecting computational nodes.

Hence, edge-base data structure and algorithm are applied to improve the efficiency of computations on unstructured meshes. Using this technique, the effects of convective and dissipative fluxes at boundary edges between two control volumes are computed once, and then, it is added to central nodes of the left and right control volumes. Similarly, the computations of artificial dissipation operators are performed on each edge, and the results are accumulatively stored for two end nodes of the edges (as control volume centre).

Note that edge-base data structure for the mesh information, in which the two end nodes as well as the left and right nodes of each edge are defined, is the main requirement of this technique [35].

6. BOUNDARY CONDITIONS

Two types of boundary conditions are applied in this work.

6.1. Flow boundary conditions

Several types of flow boundary conditions are used in this work. For sub-critical channel flow problem (with certain inflow and outflow boundaries like the test case of frictionless canal with sudden expansion in the following sections), velocity components (or discharge) and water depth

DOI: 10.1002/fld

are imposed at upstream and downstream, respectively. In such a case all the remaining flow parameters have to be extrapolated from inside the computational domain [36].

The tidal flow boundary condition (like outer boundary of the like the outer boundary of the quadrant test case or Hurmoz strait of Persian Gulf application case in the following sections) can be applied by imposing the water surface level fluctuations at tidal flow boundary (Figure 1). For such a boundary, the velocity components are extrapolated from the computational domain (using the value of computed velocity components at nodes close to the boundary). For the quadrant test case a sinusoidal fluctuation is imposed at the tidal flow boundary.

For the river inflow boundary (like Arvand River at the north-west of Persian Gulf), the annual average inflow velocity (or unit discharge q) can be imposed at that boundary. In such a case, water surface elevation at river boundary has to be extrapolated from the computational domain. In such a case, the value of computed depth at nodes close to the river boundary is used for the extrapolation.

6.2. Wall boundary conditions

Free-slip velocity condition walls can be imposed where no flow passes through the vertical plane of the flow domain. This is the condition for straight borders of the first test case. These boundaries can be used to reduce the computational domain due to symmetric conditions in radial walls of the first test case. At these boundaries the component of the normal velocities are set to zero. Therefore, tangential computed velocities are kept using free slip condition at wall boundaries.

No-slip boundary conditions can be imposed at rough wall boundaries. The vertical walls of the second test case are applications of this type of wall boundary conditions. At these boundaries all velocity components are set to zero.

Neglecting the tidal flats along the coastal zones and island boundaries in the Persian Gulf application case, free slip boundary condition can be assumed for the border line between the tidal flats and the computational domain. However, small water depths in coastal zones of the Persian Gulf may give rise to the global bed shear stresses and reduce the computed velocities in these regions.

7. GEOMETRICAL MODELLING

The coastal boundary and the bed surface topography of the Persian Gulf is very irregular and several islands of various sizes and shapes are spread over the region. A numerical model is not able to simulate the real world flow pattern unless the geometrical characteristics of flow domain (i.e. the irregularities of coasts and islands) are modelled precisely. Thus, the numerical flow solver should handle the geometrical complexities of the bed and boundaries of the flow domain. In order to overcome the problem, in the present work, attempt has made to solve the depth-averaged hydrodynamic equations on unstructured finite volumes. Application of unstructured mesh facilitates considering the effects of geometrical irregularities of coasts and islands.

The three-dimensional surface of flow bed is modelled in two stages. In the first stage, horizontal geometry of the problem is modelled by definition of some boundary curves, and then, the flow domain is discretized using unstructured mesh generated by Deluaney triangulation technique [37]. In the second stage, for converting the two-dimensional mesh (Figure 3(a)) into a three-dimensional surface (Figure 3(b)), the bed elevation of the flow domain is digitized at a number of points along

DOI: 10.1002/fld

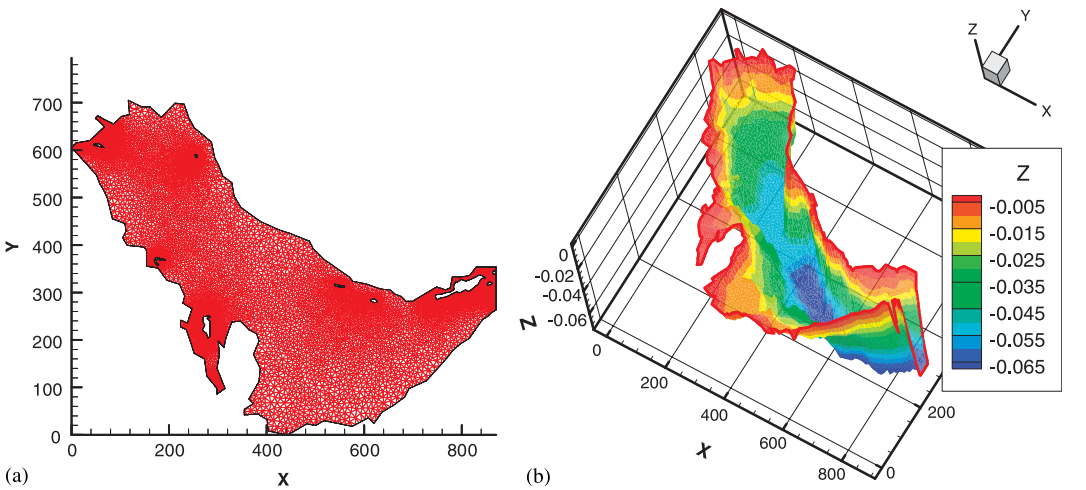

Figure 3. Discrete geometrical model for Persian Gulf: (a) two-dimensional plane mesh and (b) three-dimensional surface ($z = 0$ is mean water surface level).

some contour lines. Then, the bed elevation is set for the every node of the mesh by interpolation of the elevations of surrounding digitized points.

8. VERIFICATION TEST CASES

The major factors influencing tidal currents in Persian Gulf are tidal fluctuations in Hurmoz strait, variable bed elevations and irregularities of coastal boundaries. Hence, in this section, firstly the hydrodynamic model is examined for fluctuating (transient) flow on the variable bed elevation and the numerical results are compared with available analytical solution. Secondly, the accuracy of the model to simulate circulating deep flow in a canal with sudden expansion is assessed by comparing numerical results with the reported experimental measurements.

8.1. Fluctuation in a quadrant with variable bed elavation

The test case of tidal fluctuations in a quadrant with a parabolic bed can be used to evaluate the performance of the numerical model for solving two-dimensional flows on a bed with variable elevation which originated from a tidal boundary condition [38].

The boundary conditions are considered as follows:

$$\begin{aligned} \frac{\partial \xi}{\partial r} &= 0, \quad r = r_1 \\ \xi(r_2, \theta, t) &= Re[\xi_0(\theta) e^{i\omega t}], \quad r = r_2 \\ \frac{\partial \xi}{\partial \theta} &= 0, \quad \theta = 0, \pi/2 \end{aligned} \tag{8}$$

DOI: 10.1002/fld

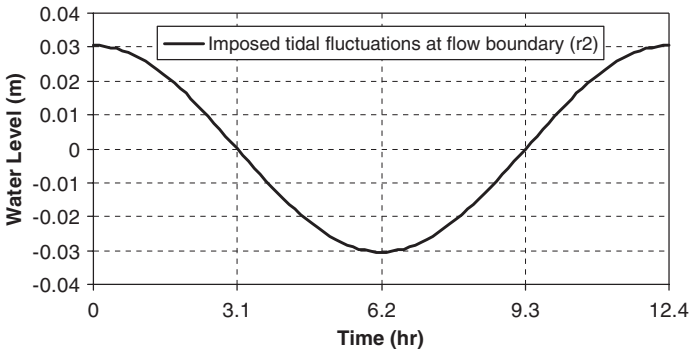

Figure 4. Sinusoidal water elevation fluctuations imposed at quadrant flow boundary.

The parameters are defined as follows: θ is the angle in polar coordinate, t the time, ξ the water elevation above mean water level, ξ_0 the tide amplitude and ω the angular frequency of tidal function. The analytical solution of ξ is given as [38]

$$\xi(r,t) = Re\left\{ \xi_0 \frac{\cos\left[\frac{\beta}{2}(r^2 - r_1^2)\right]}{\cos\left[\frac{\beta}{2}(r_2^2 - r_1^2)\right]} e^{i\omega t} \right\}, \quad \beta^2 = (\omega^2 - i\omega\tau)/gH_0 \tag{9}$$

Here, the parameters are as follows: g is the gravity, H_0 the real and constant number ($h = H_0 r^{-2}$) and τ the bed friction constant. However, in order to investigate the effects of the variable bed elevation on tidal flow, the case in the present paper is considered with negligible bed friction. Sinusoidal water elevation fluctuations are imposed at flow boundary (outer arc of the quadrant), as plotted in Figure 4.

In this work, the geometry of the quadrant is formed by considering internal radius $r_1 = 60\,960$ m, external radius $r_2 = 152\,400$ m and bed depth variation from water mean level $h = 2.5 \times 10^{12}/r^{-2}$.

In order to perform numerical simulations, the domain is discretized with triangular unstructured mesh which contains 1083 nodes, and 1989 cells and then the bed elevations are implemented to nodal points of the mesh (Figure 5). The flow patterns are computed, by imposing sinusoidal wave with amplitude of 0.3048 m and period of 12.4 h at outer arc (flow boundary).

The results of the model and the analytical solution are compared in Figure 6, for two certain times. Error analysis shows that the average and maximum error in prediction of surface water level are 0.24 and 2.1%, respectively, and for the computed velocity components the average and maximum error are calculated 1.3 and 6.9%, respectively.

8.2. Recirculation in a frictionless canal expansion

The test case of a channel with a sudden expansion (in a side wall) is chosen for verification of the numerical model for solving the circulations in deep flow due to the irregularities of wall boundary. The negligible bed friction effect provokes suitable condition for the assessment of the turbulent model effect on the accuracy of the results.

DOI: 10.1002/fld

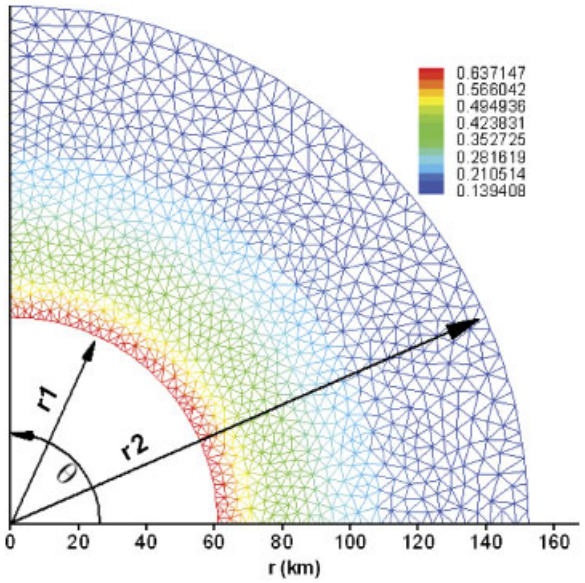

Figure 5. Geometric details of quadrant flow field (three-dimensional bottom surface mesh).

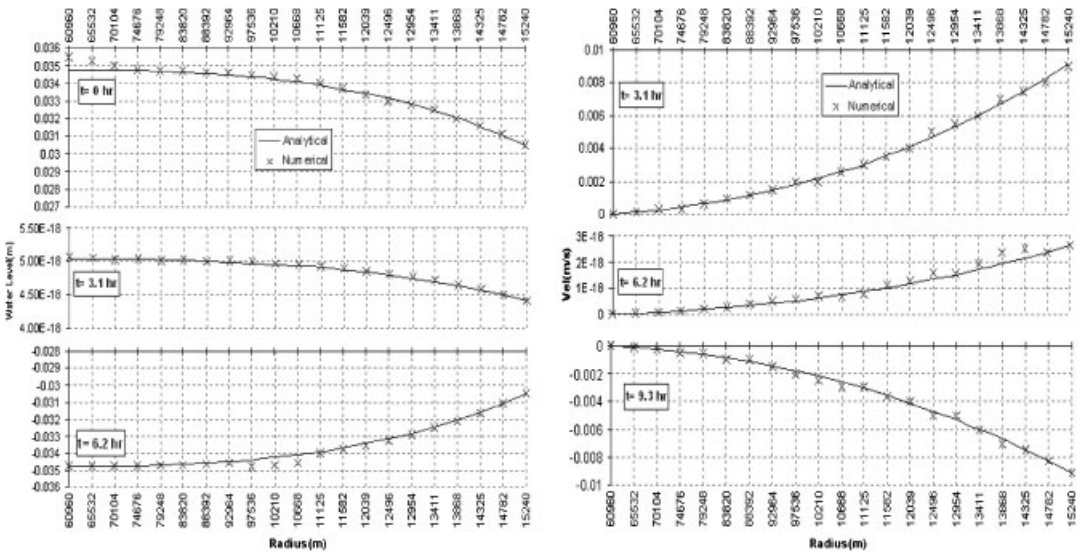

Figure 6. Comparison between numerical results (water level and velocity) and analytical solution for quadrant flow field.

DOI: 10.1002/fld

The channel width is 2 m before and 3 m after the expansion section. The inflow and outflow boundaries are the left side right side of the canal. Before the expansion part of the canal the mean velocity is 0.5 m/s and the flow depth is 1 m [39].

The domain is discretized with triangular unstructured mesh, which contains 1352 nodes and 2465 cells and local mesh refinement is imposed near the canal expansion (Figure 7). No-slip boundary condition is imposed on the side walls. At upstream flow boundary of the canal x direction velocity is imposed.

Considering bed friction number as $S = C_f d/2h$ (where d stands for the width of the channel, h for depth of water, g for gravitational acceleration, n for Manning's coefficient and C_f is friction factor), for $S < 0.05$ the current can be assumed deep and the effect of bed friction is negligible [40].

For the laboratory flume of the case (made of Plexiglas with $n = 0.0089$, $d = 3$ m and $h = 1$ m) $S = 0.0011$, and therefore, the current is deep and the bed friction effect is negligible.

As shown in Figure 8, streamline circulation is formed after expansion. The length of recirculation region is approximately 4.1 m which is very close to the experimental measurement of 3.95 m (which shows 3.8% error in computed results).

Table I shows the average and maximum error in computed velocity for three sections. The errors are calculated using the ratio of difference between numerical and experimental results to experimental data. As can be seen in Figure 9, the numerical results of steady-state velocity profiles are in a close agreement with experimental data in the three cross sections.

The maximum value of the errors computed are from near the side walls of the Section 3. This is due to the coarseness of the grid spacing at the regions where the boundary layer forms due to implementation of non-slip boundary condition (zero velocity). Since, evaluation of the computation for the flow with recirculation (due to irregularities of the wall boundaries) is the

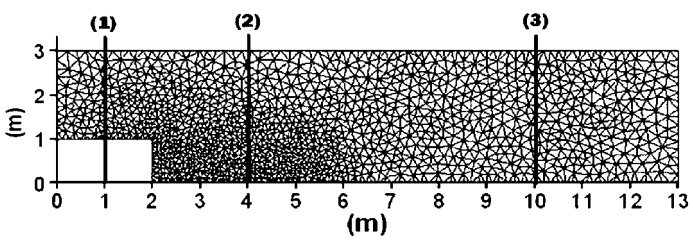

Figure 7. The triangular mesh of side-wall expansion channel and position of the sections.

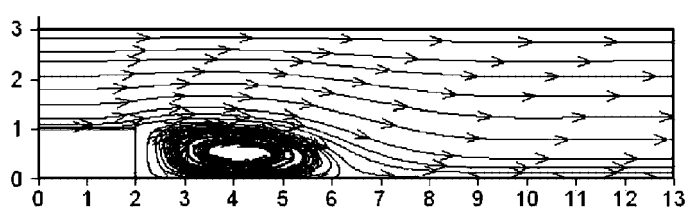

Figure 8. Stream lines and recirculation region downstream of the side-wall expansion.

DOI: 10.1002/fld

Table I. The amount of velocity error in each section in the expansion canal.

	Section 1	Section 2	Section 3
	($x = 1$ m)	($x = 4$ m)	($x = 10$ m)
Average error (%)	3.7	4.8	7.2
Maximum error (%)	9.1	10.6	15.1

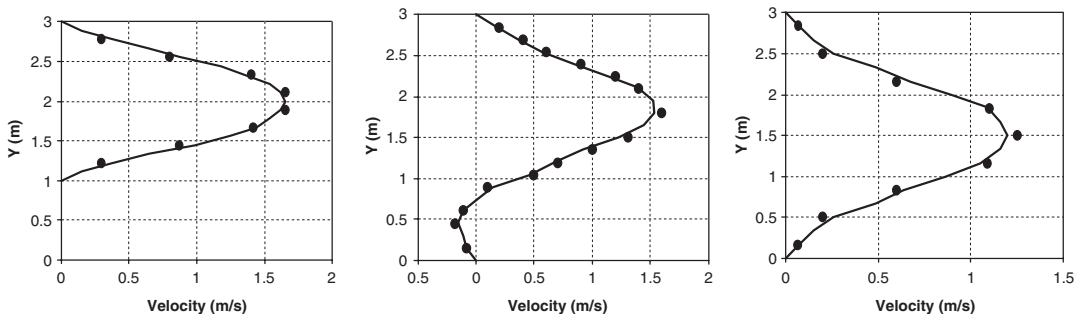

Figure 9. Comparison between numerical velocities (lines) and experimental (symbols) data at three sections; 1, 4 and 10 m from the inflow boundary of the canal, respectively.

main goal of this test case; these regions are not of major interest to the present work. The maximum value of the errors is decreased when the mesh size is reduced. Therefore, for the cases in which accurate computation of flow velocities close to the rough boundaries is important, using a fine mesh close to the no-slip wall boundaries or imposing wall function may help reducing the error at the expense of excessive computational work load.

9. REAL WORLD APPLICATION

In the previous sections, quality of the computed depth and velocity components by the developed finite volume flow-solver were assessed for geometrically simple tidal and circulating flow test cases. In this section, the ability of the model to handle a geometrically complex application case is presented by simulation of tidal currents in the Persian Gulf domain.

9.1. Modelling conditions

The discrete geometry of the Persian Gulf is modelled by generating a triangular unstructured mesh between the boundary curves along the coast lines. This mesh contains 7288 nodes, 13 532 elements, and 20 828 edges (Figure 3(a) and (b)), is refined at flow boundaries and close to the islands using point and line sources for mesh spacing.

DOI: 10.1002/fld

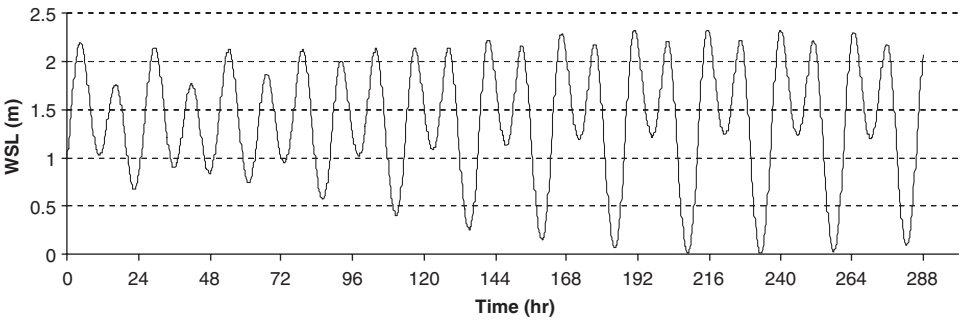

Figure 10. Water surface level fluctuations at Didamar island (Hurmoz strait) imposed at tidal flow boundary.

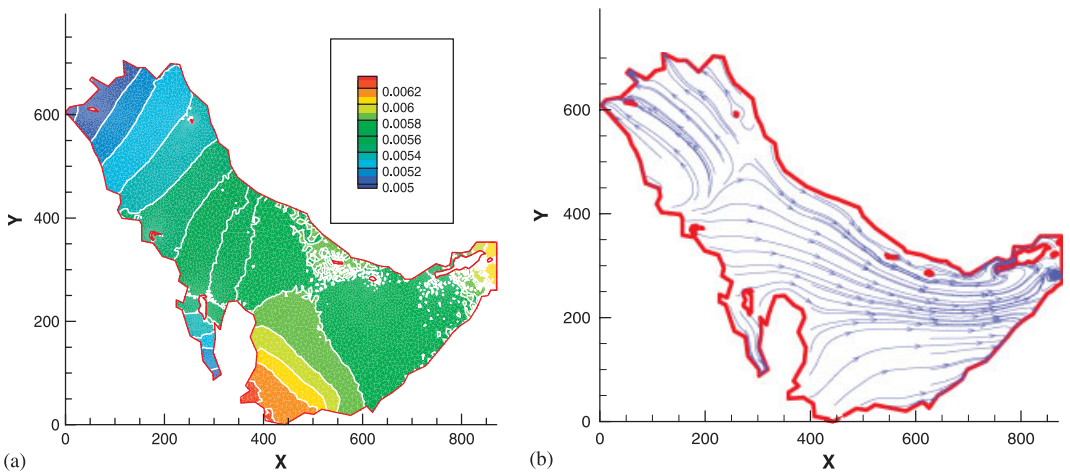

Figure 11. Typical computed results in two arbitrary times (all dimensions in kilometres): (a) water surface elevation (from mean sea level) and (b) stream traces.

In order to impose the tidal flow boundary condition at this strait, the required data for water surface fluctuations in desired period of time was obtained from Admiralty tide tables. These data were obtained from harmonic analysis; its constants are calibrated for the Didamar island, close to Hurmuz strait, by British Admiralty [24].

Tidal fluctuations of water surface elevation at east flow boundary of the Persian Gulf, which are evaluated using the predictions of tide tables at the Didamar island for a certain period of time, are plotted in Figure 10.

Note that the large diurnal inequality in the tidal signals obtained from the Admiralty tide table is mainly because of regional conditions which are considered in calibration of harmonic analysis near Didamar island by the British Admiralty.

DOI: 10.1002/fld

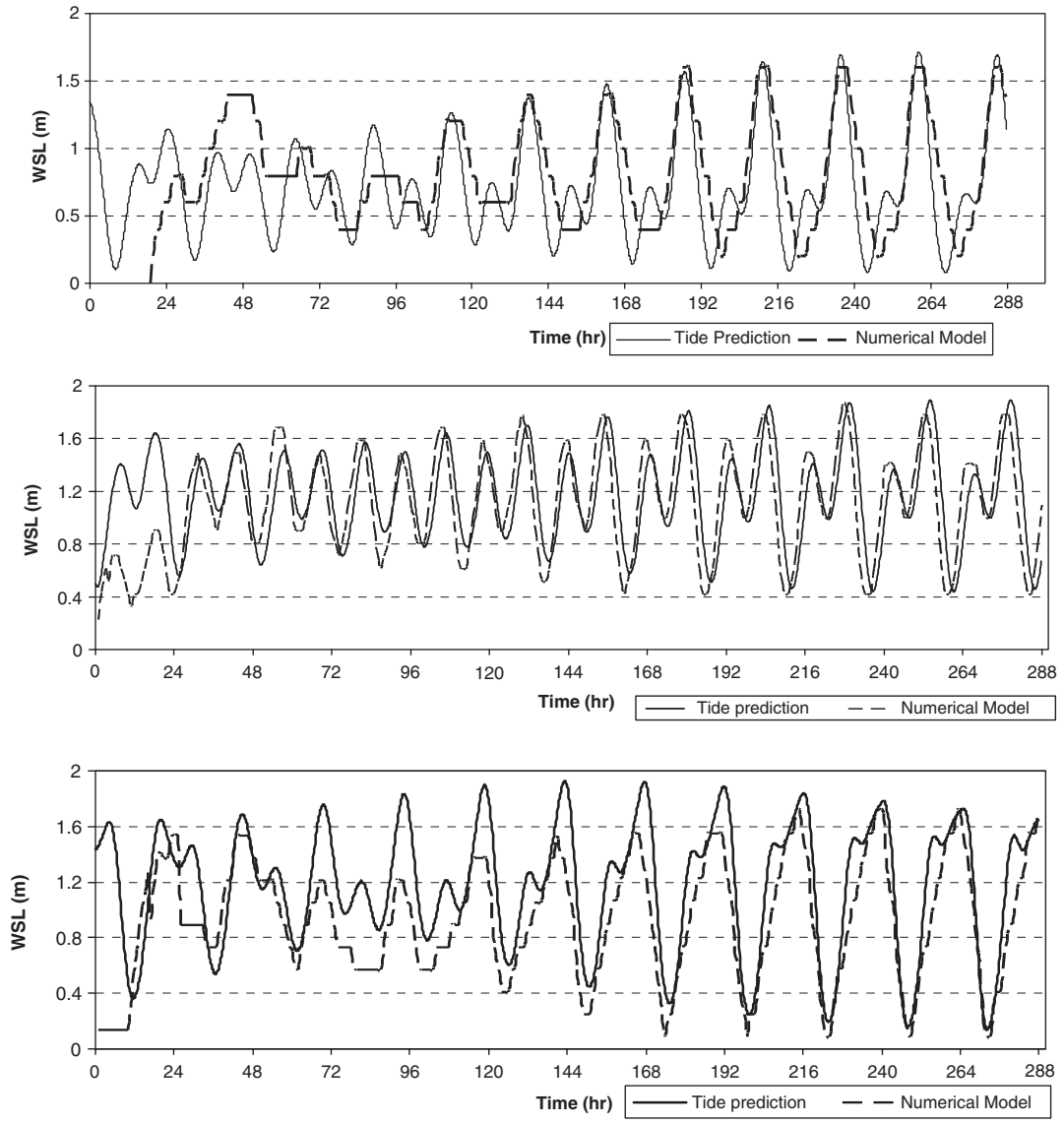

Figure 12. Comparison of the computed water surface level with the results of the British Admiralty tide table at Bushehr (Up), Ajman (Middle) and Ras-Al-Khafij (Down).

The Arvand river with average annual discharge of 136 km^3 is the major river in the Persian Gulf field. The monthly averaged inflow rate of the Arvand river (report on rainfall and surface currents in Iran, 2003) is applied for calculation of nodal normal velocities as the river inflow boundary condition. Note that the inflow from Arvand river is much less than the annual inflow from the Hormuz strait (which forms due to the evaporation from the water surface), and therefore, may have minor influences on the results of tidal flow modelling.

DOI: 10.1002/fld

Table II. Explanations and error analysis of water level alterations for each port.

Port name	Port no.	Position	Average error (%)	Maximum error in time difference of the flow tides (%)	Maximum error in time difference of the ebb tides (%)	Maximum error of the flow tides (%)	Maximum error of the ebb tides (%)
Bushehr	4283	28°54′N 50°45′E	2.3	2.8	9.7	6.9	4.2
Ajman	4204	25°25′N 55°26′E	1.6	2.3	5.5	5.5	1.8
Ras-Al-Khafji	4260 D	28°25′N 48°31′E	2.2	8.1	1.3	5.8	5.1

In shallow coastal water bodies like an embayment, estuaries, lagoons and such, experiencing tidal oscillations of the free surface, the extent of areas subjected to alternating wet and drying (the so-called tidal flats) may be of the same order of magnitude as constantly submerged areas [41]. However, in the present work, the average slope along 2650 km coastal is about 0.0011, and therefore, the average volume of water that may be stored in the tidal flats due to average 2.5 m tidal oscillation of surface water is about 7.6 km^3. On the other hand, considering the average 2.5 m tidal oscillation and average area of 237 607 km^2, the average volume of the changes in water volume of the Persian Gulf due to tidal oscillations is about 594 km^3. While the storage potential of the tidal flats is less than 1.3% of the total volume of the flow domain variations, it can be stated that ignoring tidal flats does not have considerable importance in the present modelling.

Therefore, by ignoring tidal flats, free slip wall boundary condition is considered along the coast lines and only the component of velocity vector normal to the coastal boundary edges are set to zero and computed tangential velocities are kept intact.

Considering negligible wind velocity, the flow patterns in the Persian Gulf are formed due to tidal fluctuations at east flow boundary, evaporations from the water surface, Coriolis effects, the coasts and bed surface geometry and roughness. The flow patterns computed by the hydrodynamic model of the Persian Gulf can be presented in terms of water surface elevations and stream traces (Figure 11(a), (b)).

9.2. Modelling results

In this section, the present model (that its accuracy is assessed in previous section) is applied for modelling tidal currents in the Persian Gulf. Since the authors have no access to the field measurements of current velocities, the quality of the results is assessed only by comparing the computed water surface elevation (thick line) with the calibrated harmonic analysis predictions of the Admiralty tide table (thin line) at Bushehr (I.R.Iran), Ajman (United Arab Emirates) and Ras-Al-Khafij (Kuwait) ports (Figure 12).

For this simulation, the tidal fluctuations at Didamar island, for the period of 12 days from December 2003 (Figure 10), are imposed at Hurmoz strait. Still water is considered at the start of the computations, and hence, after a few days warm up period, the results of the hydrodynamic model are compared with the Admiralty tide table predictions. Therefore, the computed flow

DOI: 10.1002/fld

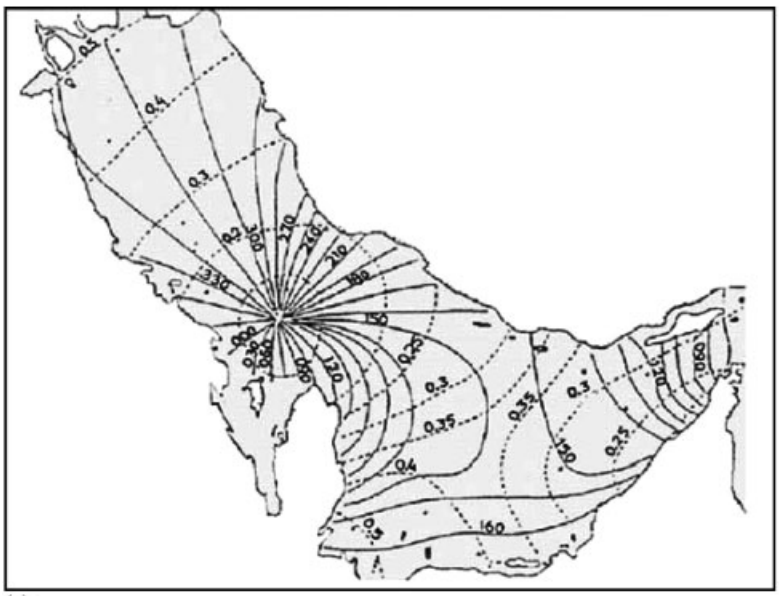

(a)

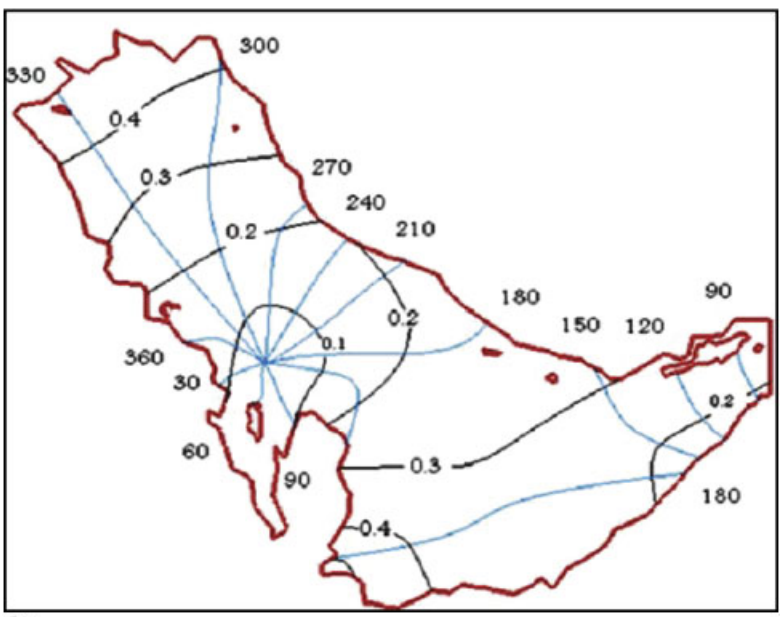

(b)

Figure 13. Comparison between co-tidal charts for the K_1 harmonic constituent amplitude counters (m) and phase counters (degrees): (a) British Admiralty reproduced by Danish Hydraulic Institute [19] and (b) present model results.

DOI: 10.1002/fld

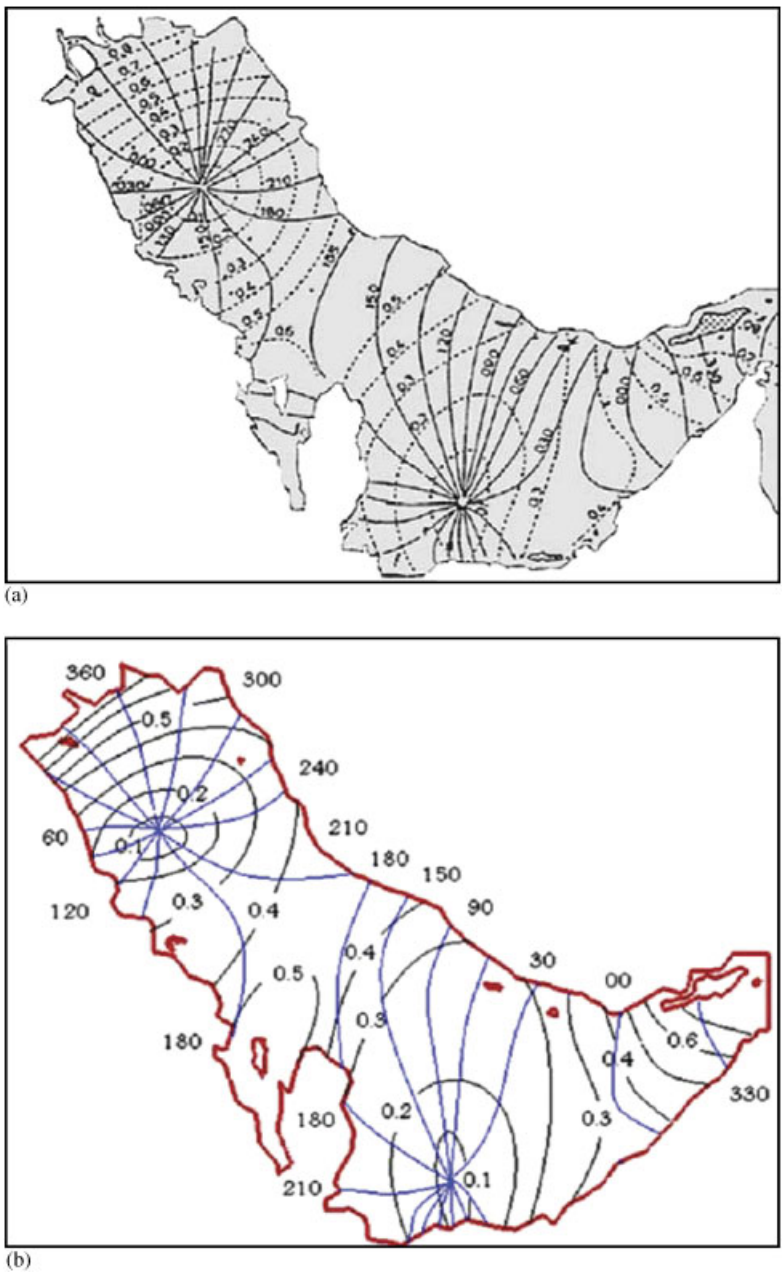

Figure 14. Comparison between co-tidal charts for the M_2 harmonic constituent amplitude counters (m) and phase counters (degrees): (a) British Admiralty reproduced by Danish Hydraulic Institute [19] and (b) present model results.

DOI: 10.1002/fld

parameters during the second week of computations can be used for the assessment of the quality of the results. During this period, the average and the maximum errors for the water elevations as well as time difference for prediction of the ebb and flow of tide are tabulated for Bushehr, Ajman and Ras-Al-Khafij Ports (Table II).

The source of errors might be incomplete geometry modelling (simplification on coastal and bed irregularities as well as ignoring several small islands, particularly along the coastal zones), the relatively coarse mesh spacing (about 5 km) which do not cover all the geometrical details, ignoring the effect of tidal forces on water bodies inside the Persian Gulf, considering average annual evaporations instead of actual evaporations for the desired period of time, ignoring wind effect (particularly along the coastal zones near Bushehr, Ras-Al-Khafji and Al Jubayl ports) and the most important one, variable roughness for a long distance (e.g. more than 700 km between Hurmoz strait and Bushehr port, with very rough surface along the beach). Therefore, the present model may produce more accurate results by considering more geometrical complexities and calibration of field parameters (such as bed roughness and climatologically precise data for desired time).

9.3. Computing tidal constituents

This section presents the results of the present model in terms of the two most important tidal constituents; K_1 (lunisolar diurnal constituent) and M_2 (principal lunar semidiurnal constituent). M_2 represents the relation of earth with respect to the moon, for a period of 12.42 h and K_1 expresses the effect of the moon's declination, for a period of 23.93 h [42]. The computed results are compared with the values tabulated in Admiralty tide tables. In order to produce plots of the present model results, fast Fourier transform (FFT) was utilized. The resulted co-tidal charts for amplitude and phase counters are shown in Figures 13 and 14.

10. CONCLUSIONS

The numerical analyser for scientific and industrial requirements (NASIR) hydrodynamic model solves the time dependent depth-averaged equations of continuity and motions considering overlapping finite volumes formed in a three-dimensional triangular surface mesh which preserves the geometrical complexities of variable bed topography. The numerical results of fluctuating flow in a quadrant variable bed elevations presents acceptable agreements with the analytical solution of the velocity field as well as the water surface fluctuations. The numerical results of the developed model for simulation of two-dimensional turbulent circulating flows in a channel expansion with negligible bed friction effects demonstrate good agreements with reported experimental measurements for two-dimensional circulations in deep waters. As a sample application of the developed model to solve flow patterns in a geometrically complex domain, the tidal currents in Persian Gulf are modelled, considering tidal fluctuations at flow boundary, inflow from a river, evaporations and Coriolis effects, bed surface geometry and roughness. The results of the tidal current simulation are assessed by comparison of the computed water level at three ports and the Co-tidal charts for the K_1 and M_2 in Persian Gulf with British Admiralty tide table. The results of the NASIR shallow water flow solver for the verification test cases present promising agreements, and computed flow patterns for the Persian Gulf tidal currents encourages application of the developed flow solver for more detailed simulations by considering more geometrical complexities and calibration of field parameters.

DOI: 10.1002/fld

REFERENCES

1. Ezer T, Mellor GL. Sensitivity studies with the North Atlantic sigma coordinate princeton ocean model. *Journal of Dynamics of Atmospheres and Oceans* 2000; **32**:185–208.
2. DHI, Water and Environment. Modelling the world of water, Product catalog, 2005.
3. Neill SP, Copeland GJM, Folkard AM. Dynamics of tidal fronts in the Tay Estuary, Scotland. *Tenth Annual Conference on Physics of Estuaries and Coastal Seas Norfolk*, Virginia, 2000.
4. Young DL, Lin QH, Murugesan K. Two-dimensional simulation of a thermally stratified reservoir with high sediment-laden inflow. *Journal of Hydraulic Research* 2005; **43**(4):351–365.
5. Al-Rabeh AH, Gunay N, Cekriege HM. A hydrodynamic model for wind-driven and tidal circulation in the Arabian Gulf. *Journal of Applied Mathematical Modelling* 1990; **14**:410–419.
6. Swift MR, Brown WS. Distribution of bottom stress and tidal energy dissipation in a well-mixed estuary. *Estuarine Coastal and Shelf Science* 1983; **17**:297–317.
7. Bilgili A, Swift MR, Lynch DR, Ip JTC. Modelling bed-load transport of coarse sediments in the Great Bay Estuary, New Hampshire. *Estuarine*, *Coastal and Shelf Science* 2003; **58**:937–950.
8. *Ocean Circulation and Plume Dispersion Modelling Review, with Emphasis on Orange County Sanitation District's Offshore Outfall and Wastewater Plume.* Orange County Sanitation District, Lafayette, CA, TETRA TECH, Inc., 2000.
9. Shchepetkin AF, McWilliams JC. The regional oceanic modelling system (ROMS): a split-explicit, free-surface, topography-following-coordinate oceanic model. *Journal of Ocean Modelling* 2005; **9**:347–404.
10. McLaughlin JW, Bilgili A, Lynch DR. Numerical modeling of tides in the Great Bay Estuarine System: dynamical balance and spring-neap residual modulation. *Estuarine Coastal and Shelf Science* 2001; **57**(1–2):283–296.
11. Egbert GD, Erofeeva SY. Efficient inverse modeling of barotropic ocean tides. *Journal of Atmospheric and Oceanic Technology* 2002; **19**:183–204.
12. Chen C, Liu H. An unstructured grid, finite-volume, three dimensional, primitive equations ocean model: application to coastal ocean and estuaries. *Journal of Atmospheric and Oceanic Technology* 2003; **20**:159–186.
13. Von-Trepka L. Investigation of the tides in the Persian Gulf by means of a hydrodynamic numerical model. *Proceeding of Symposium on Mathematical Hydrological Investigations of Physical Process in the Sea*, Inst. Fur Meer. Der Univ. Hamburg., vol. 10, 1968; 59–63.
14. Lardner RW, Belen MS, Cekirge HM. Finite difference model for tidal flows in the Arabian Gulf. *Computers and Mathematics with Applications* 1982; **8**(6):425–444.
15. Chu WS, Baker BL, Akbar AM. Modeling tidal transport in Arabian Gulf. *Journal of Water Way*, *Port*, *Coastal and Ocean Engineering* 1988; **114**(4):455–471.
16. Evans-Roberts DJ. Tides in Persian Gulf. *Consulting Engineer* 1979; **43**(6):46–48.
17. Hunter JR. Tidal and stratification-mixing models of Kuwait waters. *Kuwait Bulletin of Marine Science* 1984; **5**:11–35.
18. Proctor R, Elliot AJ, Flather RA. Prediction and observation of the Arabian Gulf oil slick. *Journal of Nitride Semiconductor* 1992; **17**(4):215–227.
19. Najafi HS, Noye BJ, Teubner MD. Spherical-coordinate numerical model of the Persian Gulf. *Computational Techniques and Applications CTAC-95* 1995.
20. Technical standards and commentaries for port and harbour facilities in Japan, The overseas coastal area development institute of Japan, 2002.
21. Schott F, McCreary Jr JP. The monsoon circulation of the Indian Ocean. *Progress in Oceanography* 2001; **51**(1):1–123.
22. Wilkinson BH, Drummond CN. Facies mosaics across the Persian Gulf and around antigua—stochastic and deterministic products of shallow-water sediment accumulation. *Journal of Sedimentary Research* 2004; **74**: 513–526.
23. Yakhot V, Orszag SA, Thangam S, Gatski TB, Speciale CG. Development of turbulent model for shear flows by a double expansion technique. *Physics of Fluids A* 1992; **4**(7):1510–1520.
24. Admiralty tide tables, British Admiralty, 1964.
25. Vreugdenhil CB. *Numerical Methods for Shallow Water Flow*. Kluwer Academic Publisher: Dordrecht, 1994.
26. Castanedo S, Medina R, Mendez FJ. Models for the turbulent diffusion terms of shallow water equations. *Journal of Hydraulic Engineering* (ASCE) 2005; **131**:217–223.
27. Smagorinsky J. General circulation experiments with the primitive equations. Part I: the basic experiment. *Monthly Weather Review* 1963; **91**:99–152.

DOI: 10.1002/fld

28. Nadaoka K, Yagi H. Shallow-water turbulence modeling and horizontal large-eddy computation of river flow. *Journal of Hydraulic Engineering* 1998; **124**(5):498–500.
29. Rodi W. *Turbulence Models and Their Applications in Hydraulics* (3rd edn), IAHR Monograph. Balkema: Rotterdam, Netherlands, 1993.
30. Jia Y, Wang SSY. Numerical model for channel flow and morphological change studies. *Journal of Hydraulic Engineering* (ASCE) 1999; **125**(9):924–933.
31. Wu W. Depth-averaged two-dimensional numerical modelling of unsteady flow and non-uniform sediment transport in open channels. *Journal of Hydraulic Engineering* (ASCE) 2004; **130**(10):1013–1024.
32. Jameson A, Baker TJ, Weatherill NP. Calculation of inviscid transonic flow over a complete aircraft. *AIAA 24th Aerospace Science Meeting*, Reno, Nevada, *Paper-86-0103*, 1986.
33. Gottlieb S, Shu C-W, Tadmor E. Strong stability-preserving high-order time discertization methods. 2001; **43**:89–112.
34. Enander R, Karlsson AR. Implicit explicit residual smoothing in multi-grid cycle. *AIAA 33rd Aerospace Sciences Meeting and Exhibit*, Reno, Nevada, vol. 95, 1995; 0204.
35. Mavriplis D. Unstructured mesh related issues in computational fluid dynamics (CFD)-base analysis and design. *Eleventh International Meshing Roundtable*, Ithaca, New York, U.S.A., 2002.
36. Sabbagh-Yazdi SR, Mohammadzadeh-Qomi M. Finite volume solution of two-dimensional convection dominated sub-critical flow using unstructured triangular meshes. *International Journal of Civil Engineering* 2004; **2**(3): 78–91.
37. Thompson JF, Soni BK, Weatherill NP. *Hand Book of Grid Generation*. CRC Press: New York, 1999.
38. Chen CL. Analytic solution for tidal model testing. *Journal of Hydraulic Engineering* (ASCE) 1989; **115**(12): 1707–1714.
39. Denham MK, Patrick MA. Laminar flow over a downstream facing step in a two dimensional flow channel. *Transactions of the Institute of Chemical Engineers* 1974; **52**:361–367.
40. Babarutsi S, Chu VH. Modelling transverse mixing layer in shallow open channel flows. *Journal of Hydraulic Engineering* (ACSE) 1989; **124**:643–659.
41. Balzano A. Evaluation of numerical simulation of wetting and drying in shallow water flow models. *Coastal Engineering* 1998; **34**:83–107.
42. Shurman P. Manual of harmonic and analysis and prediction of tides. 1958 (reprinted).

DOI: 10.1002/fld